Chapter 8

Applications in space physics

Space physics is the scientific discipline which studies the physical processes that are at work in our solar system and in the coupled solar-terrestrial system. Processes in the earth's magnetosphere and phenomena in the solar corona are important topics of research, and the knowledge gained from studying these topics may help us to understand the connection between solar activity and perturbations of the earth's magnetic system or 'space weather'.

Newly discovered physics regarding complex MHD shock phenomena in a magnetically dominated medium has been described in the previous Chapters. The discussion in these previous Chapters was set in an abstract context, which enabled us to concentrate on the basic physical effects and to state the results in all their generality. In the present Chapter we leave this abstract setting and we apply what we learned about MHD shocks to plasma flows with shocks in the solar system. The new results on MHD shocks may also have applications in astrophysical plasma flows beyond our solar system. This is not addressed in this dissertation, but certainly remains an interesting and unexplored research topic.

Shocks are ubiquitous in space physics plasma flows and shock phenomena play an important role in space weather. The supersonic and super-Alfvénic solar wind generates a bow shock in front of the earth [114], which forms the transition between the solar wind flow and the earth's magnetosphere. Strong shocks are generated in front of solar coronal mass ejections (CMEs) when CMEs leave the corona at super-Alfvénic speeds [68]. These CMEs propagate in the solar wind through the interplanetary medium, and their leading shocks are observed by space probes as interplanetary shock waves. Some of the CMEs that

reach the earth have been observed *in situ* as magnetic clouds with a preceding shock [15, 58]. The interaction of such a shock–cloud structure with the earth's bow shock and magnetosphere can generate violent perturbations of the earth's magnetic system called magnetic storms. Magnetic storms can adversely affect satellites, communication systems and power grids on the earth, and resulting failures are referred to as the effect of 'space weather'.

In this Chapter we present two examples of space physics plasma flows with shocks for which the newly discovered intrinsically magnetic effects on bow shock topology are important. In Sec. 8.1 we discuss complex shock phenomena induced by fast solar CMEs. In Sec. 8.2 we apply the new results on MHD shock topology to the bow shock generated by the interaction of the solar wind with the earth and its magnetic system. Remark that the secondary shock in the magnetically dominated bow shock topology (Fig. 7.1) is of intermediate, slow switch-off or slow type depending on the exact location along the shock front. For definiteness we refer to the secondary shock front as a secondary *slow* shock front in this Chapter.

8.1 Shocks induced by fast CMEs

We begin this Section with a brief overview of some properties and observations of the solar corona and CMEs. Then we discuss if the magnetically dominated shock topology described in Chap. 7 may arise when fast CMEs generate preceding shock fronts, and we ask ourselves whether those multiple interacting shocks could be observed with present-day observational means.

8.1.1 Coronal mass ejections

Up to several times per day, large-scale structures in the solar corona disrupt and are ejected out of the corona at speeds ranging from 10 to 2×10^3 km/s, carrying a mass of 10^{12-13} kg and liberating an energy of 10^{24-25} J [66, 104, 68]. The propagation of CMEs in the highly ideal solar coronal plasma may be described by the equations of ideal MHD. CMEs are ejected into interplanetary space from low in the solar corona where magnetic forces dominate over thermal pressure forces, such that the plasma β is substantially smaller than $2/\gamma = 1.2$. Switch-on shock phenomena can arise when $\beta < 2/\gamma$. Further away from the sun the solar wind becomes pressure-dominated and the plasma β rises above 1.2. This transition can be estimated to be located at around 3 solar radii (R_s) measured from the center of the sun. The solar wind is subsonic and sub-Alfvénic in the lower corona, but becomes supersonic and super-Alfvénic

at larger distances. The Alfvén speed is estimated to be 600 km/s at 3 R_s, and decreases outward as the magnetic field becomes weaker [68].

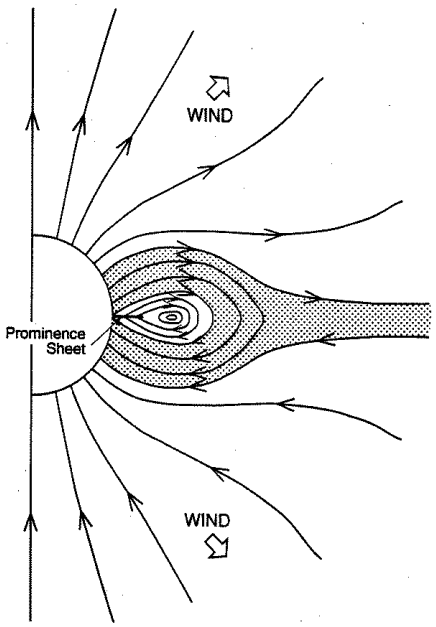

Figure 8.1: *Sketch of a hypothetical pre-CME configuration in the lower solar corona idealized to be axi-symmetric. CMEs generally occur when helmet streamers erupt. A helmet streamer is shown, which has a three-part structure: a high-density shell consisting of closed magnetic field lines rooted in the solar photosphere (shaded), a low-density cavity at the base, and a high-density prominence in the cavity (from Low (1996) [104]).*

Observations show that CMEs generally occur when arcade-like structures in the lower corona — which are called helmet streamers — erupt. We now briefly describe a theoretical model of the configuration which is believed to exist in the corona prior to CME eruption. This model is due to B. C. Low [104]. The model may not be applicable to all CMEs, but there is substantial observational evidence that a large class of CME events originate from the hypothetical pre-CME configuration sketched in Fig. 8.1. The pre-CME helmet streamer has a three-part structure: a high-density shell (seen as a bright dome-like structure in coronagraph observations) consisting of closed magnetic field lines rooted in the solar photosphere (shaded), a low-density cavity at the base, and

a high-density prominence in the cavity. Energy estimates indicate that the eruption of a helmet streamer and the ejection of the CME material must mainly be driven by magnetic energy, and this energy is presumably stored in the form of a detached flux rope of helically twisted magnetic field which forms the cavity. In realistic geometry, as opposed to the axi-symmetric idealization in Fig. 8.1, the cavity flux rope may be anchored to the coronal base at the two ends of the rope. When a CME takes off, the initially closed magnetic field lines which form the bright dome overlying the cavity open up and a current sheet is formed as a layer separating the open magnetic field lines of opposite polarities. In a later stage those magnetic fields of opposite polarities reconnect resistively low in the corona where the magnetic field dominates over the pressure, which presumably results in a solar flare and finally reformation of the helmet structure as a region of closed magnetic field.

8.1.2 Coronagraph observations

Coronagraph observations are the most important source of information on CMEs. Fig. 8.2 shows images of a CME taken by the space-borne Solar Maximum Mission (SMM) coronagraph [14], which was operational from 1980 to 1989. A coronagraph determines the electron density in the corona by measuring intensities of white light Thomson scattered by coronal free electrons. Direct light from the solar surface is blocked out by a disc covering the sun. Intensities on a coronagraph image are a direct measure of the coronal density integrated along the line of sight through the optically thin corona. This line of sight projection effect makes coronagraph images generally hard to interpret.

The SMM images of Fig. 8.2 show an erupting CME. The outer loop is seen to expand, with the bright structure closer to the sun being the prominence in the low-density cavity. In the right hand panel both the outer loop and the prominence have expanded substantially. The prominence material reveals a helical magnetic field structure. For the purpose of studying MHD shock effects induced by fast CMEs, we are now mainly interested in what happens near the leading feature of the outward moving CME. In the left panel a small 'dimple' can be seen in the leading front. In the subsequent image, taken about 16 minutes later, the dimple has become much more pronounced, and secondary bright features (indicated by arrows) following the leading front can be observed. The CME accelerates to an estimated speed of 1055 km/s [14], which is higher than the expected coronal Alfvén speed.

Fig. 8.3 shows difference images of a fast CME taken by the LASCO C3 coronagraph aboard the SOHO spacecraft [31]. SOHO became operational in 1996, and the C3 coronagraph has a much larger field of view (up to $30R_s$) than previous coronagraphs. A dimpling of the leading

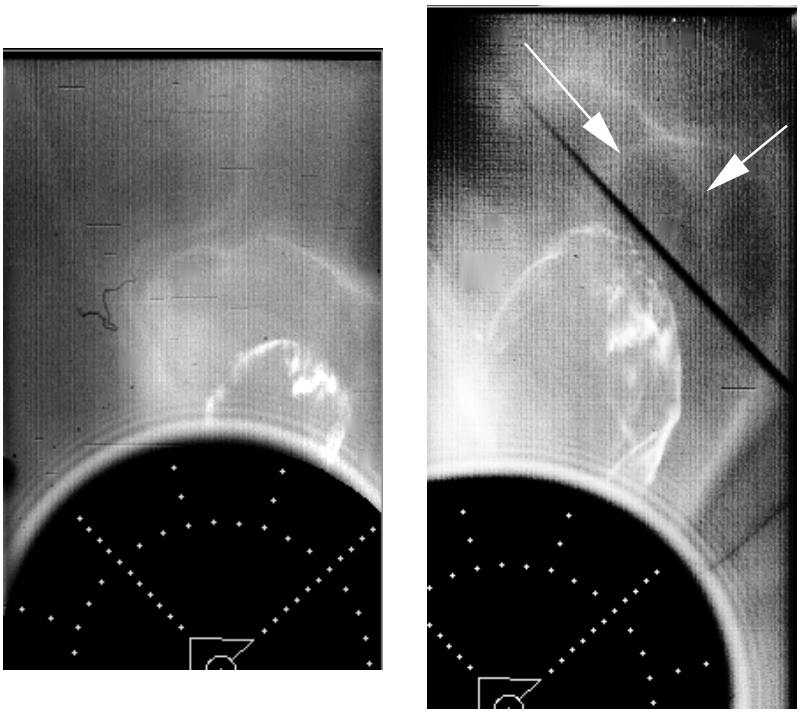

Figure 8.2: *Observation of a solar CME with the SMM coronagraph. The black disc covers the sun and has a radius of 1.6 × R_{sun}. The field of view of the SMM coronagraph stretches out to approximately 6 × R_{sun}. The images, taken on January 30, 1990, at 2:11, and 2:27 UT (from left to right), show the initial dimpling of a fast CME front and a more clearly dimpled leading front with several trailing structures (indicated by arrows) in a later stage. (Coronagraph data courtesy HAO/NCAR.)*

front can clearly be observed, and secondary features are clearly visible behind the leading front. We want to draw the attention on the conspicuous straight-line feature (indicated by the yellow arrow) which follows the leading front in the lower part of the CME, and which is consistently present in all the images.

8.1.3 CMEs and shocks

Do fast CMEs induce shocks?

There is a wide variation in the speeds with which CMEs propagate out of the solar corona. Statistical analysis of six years of SMM data [69, 68] shows that up to 20% of mass ejections move with a projected speed

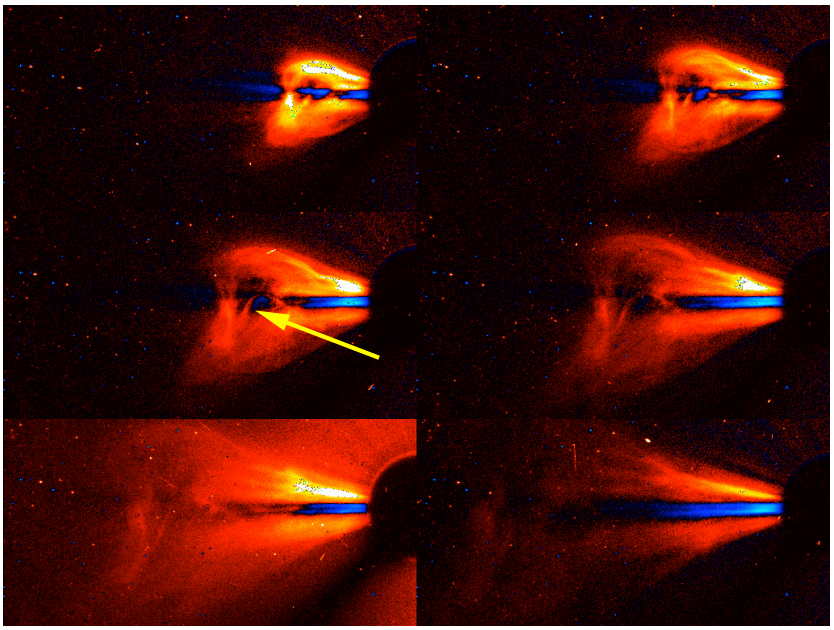

Figure 8.3: *Observation of a solar CME with the LASCO C3 coronagraph. The field of view stretches out from approximately 6 × R_{sun} to approximately 30 × R_{sun}. The images are taken on December 14, 1997, from 2:11 to 12:28 UT, and a pre-event image has been subtracted. A dimpling of the leading front can clearly be observed, and a straight-line secondary feature (indicated by the yellow arrow) is clearly visible behind the leading front. (Coronagraph data courtesy LASCO consortium.)*

which is higher than the estimated Alfvén speed. CMEs generally move outward almost radially, and the magnetic field in the solar corona is mostly radial too, so these fast CMEs move presumably faster than the fast MHD wave speed — which coincides with the Alfvén speed along the radial field lines. The solar wind speed is small in the lower corona, so many of those fast CMEs also move with superfast speeds relative to the solar wind. This means that fast CMEs (up to 20% of the total number of CMEs) move faster than the fastest wave speed in the coronal plasma. Then it follows from first-principle physical arguments (see also Chap. 2) that a shock wave must be generated in front of the moving CME. The shock forms the transition between the undisturbed superfast (in the shockframe!) upstream region and the subfast region downstream from the shock. This situation is similar to the case of an object flying through a stationary plasma with superfast speed, in which case the object is

preceded by a shock. In this sense the simulation results presented in Chap. 7 for uniform stationary MHD bow shock flows around a sphere apply also to the case of CMEs moving through the solar corona. The CME, however, is a highly time-dependent process, because the CME material can deform and expand during its outward motion, and because the upstream solar wind is not uniform. The simulation of a stationary flow around a rigid obstacle can thus only be an approximation of CME flow, and in such simulations only the aspects of MHD shock formation which are independent from the details of the downstream flow may be potentially relevant for CME propagation.

It is believed that CMEs moving outwards with a speed slower than the fast speed, but faster than the slow MHD speed, may induce preceding *slow* mode MHD shock fronts [145, 68]. This is an interesting separate topic, and the simulation results for the transition from superfast to subfast flow presented in this dissertation do no apply to this class of events.

The shocks induced by fast CMEs have been observed in space, and many observed interplanetary shock waves are believed to be associated with CMEs. The physical link between interplanetary shock waves and CMEs is, however, not always very clear. It is believed that the impulsive post-CME reconnection flare may drive blast waves to propagate into interplanetary space as shocks quite distinct from those induced by outward moving CME material. There is thus still a lot of discussion about where and how interplanetary shock waves are generated. We now briefly review some of the observations regarding shocks induced by CMEs and regarding interplanetary shock waves.

Observations of shocks induced by CMEs

There are several different sources of observational information about CME-induced shock waves.

First, in the late 70s the HELIOS satellites performed in-situ measurements as close to the sun as $10R_s$. Fast MHD shocks were observed, and there was a good correlation with fast CMEs observed by the Solwind coronagraph [136]. This was the first clear observational confirmation that fast CMEs do indeed generate fast MHD shocks.

Second, Ulysses and other heliospheric spacecraft have observed many fast MHD shocks which are believed to be associated with CMEs, at distances up to several Astronomical Units (AU) from the sun [57]. One AU is the average distance between the sun and the earth.

Third, upstream from the earth's bow shock, observations by the ACE and WIND satellites routinely show the arrival of interplanetary shocks. A magnetic cloud is a transient ejection in the solar wind defined by relatively strong magnetic fields, a smooth rotation of the magnetic

field direction and a low plasma β [15]. Magnetic clouds are believed to originate from CMEs, and they often are preceded by a shock front. The interaction of magnetic clouds with the earth's magnetic system is discussed in Sec. 8.2.3.

Radio observations are a fourth way to observe interplanetary shocks. MHD shocks produce so-called type II radio bursts [125]. The frequency of the radio signal depends on the ambient density at the emission site. Using a model for the variation of the density in the radial direction, the propagation of shock fronts can be followed all the way from the sun to the earth. Unfortunately there is a large uncertainty in the density profiles which results from the available density models so that interpretations based on these models are not unique. Radio observations seem to indicate that when fast CMEs erupt, shocks are formed well inside the field of view of coronagraphs [75].

Fifth, the most direct observations of CMEs are provided by white-light coronagraph images. From first-principle reasoning it follows that CMEs which propagate with a superfast speed relative to the ambient solar wind induce a preceding shock front, and that no perturbations can precede this shock wave. The leading feature of a fast CME in a coronagraph image can thus naturally be identified with the induced shock. However, line of sight integration effects complicate the interpretation of coronagraph images considerably. Our simulation results in Chap. 7 show that at a leading shock the post-shock density should be about a factor 2 to 3 higher than the pre-shock density. In the real corona this factor is likely to be larger due to the large heat conduction. Such a density contrast should show up in coronagraph images, but the line of sight effect would smear the discontinuous jump out into a jump not of the intensity but of the gradient of the intensity. In the strict sense, shocks — defined as discontinuous variations in intensity — can thus not readily be seen on coronagraph images. Instead, a relatively sharp transition in intensity gradient at the leading edge of a fast CME could well be a signature of a fast shock. The change in intensity gradient at the leading edge of a CME in a coronagraph image should then correspond to the expected density jump at a leading shock. Hundhausen (private communication) has analyzed the coronagraph intensity variation at leading edges of fast CMEs, and has found good agreement with the intensity variation derived from the expected density jump at preceding shocks. Leading bright edges of fast CMEs in coronagraph images can thus be interpreted as signatures of fast MHD shocks, or, more precisely, at least a portion of the bright signature may have been produced by shock compression of the ambient corona [146]. It has to be noted that there is no general agreement on this interpretation.

CMEs and multiple interacting shock fronts

In Chap. 7 it was argued that the magnetically dominated bow shock topology of Fig. 7.1 with a secondary slow shock following the leading fast shock, is independent from the details of the downstream flow, because this topology is imposed by the geometrical properties of switch-on shocks at perpendicular points on the leading shock front. In this sense we can expect that the magnetically dominated topology described in Chap. 7 may also occur in the case of shocks induced by fast CMEs, when upstream flows are magnetically dominated and switch-on shocks occur on the leading shock front. In the lower corona the plasma β is indeed likely to be lower than 1.2, the upstream magnetic field is presumably close to radial in many cases, and there must certainly be fast CMEs which move with speeds between the Alfvén speed and about two times this speed relative to the solar wind. The switch-on condition Eq. 3.77 must thus be satisfied for the shocks induced in front of these fast CMEs, and we can expect that secondary slow shocks form as in Fig. 7.1. This reasoning seems to indicate that in the lower corona secondary slow shocks should be present between the leading fast shock and the CME material in the case of fast CMEs. If those shocks are indeed formed, could we be able to detect them with present-day observational capabilities?

Let us first consider coronagraph observations. In Figs. 8.2 and 8.3 we clearly see dimpled leading fronts and secondary features following the leading fronts (indicated by arrows). The dimpling of the leading front is reminiscent of the dimpled leading shock fronts arising in our simulations of MHD bow shock flows with magnetically dominated upstream parameter values (e. g. Figs. 6.2 and 7.4). Steinolfson and Hundhausen [147] found dimpled leading shock fronts in their 2D simulation results of fast moving CMEs, and the apparent dimpling of leading features of fast CMEs in coronagraph observations has indeed been interpreted as indirect observational evidence for the occurrence of MHD switch-on shock phenomena ahead of fast CMEs [68, 147]. In our simulation results for magnetically dominated parameter values, secondary slow shocks follow the leading shock front, and the coronagraph observations do indeed suggest secondary features which have developed behind the leading bright fronts.

The secondary features indicated by arrows in Fig. 8.2 are vaguely reminiscent of the slow shocks following the leading front in the simulation result of Fig. 7.19 (first and second panel). The secondary feature indicated by the arrow in Fig. 8.3 is not unlike the secondary feature in the simulation result of Fig. 7.4a. Some coronagraph images may show evidence of the V-shaped features present in our simulation results for the transient phase of the flows (Figs. 7.19 and 7.20). Indeed, if we es-

timate the effective 'radius' of the ejected CME material to be typically 7×10^6 km (or approximately 1 R_s) and the Alfvén speed to be 600 km/s, then the simulation of Fig. 7.20 shows that the V-shaped feature is formed and convected away in the simulation on time scales of about one hour. LASCO coronagraph images are taken several times per hour, so the V-shaped feature could be observable. In fact, some observations of secondary features in CMEs [32] could be related to the simulated structure of Fig. 7.20.

Like for the dimple, we can argue that the secondary features visible in Figs. 8.2 and 8.3 may be signatures of the secondary slow shocks present in our simulation results. Of course this observational evidence is indirect and inconclusive. It is indeed not difficult to think of alternative interpretations for the secondary features in the coronagraph images, and the coronagraph observations do not seem to provide enough information to enable conclusive interpretation of features like this.

Our simulation results lead us to predict the possible observation of secondary shock-like features lagging the leading front of fast CMEs, but unfortunately present-day observational capabilities seem not to be able to identify such features conclusively. Future time-dependent 3D MHD simulations with a realistic CME structure may strengthen this prediction if they were to confirm the formation of secondary slow shocks. Line of sight integration could be performed on such simulation results to mimic coronagraph images, which could be compared with real coronagraph images. This may help in the identification of secondary slow shocks, but it is our expectation that interpretation would remain difficult and that the results might still be inconclusive. The STEREO satellites which may be launched a few years from now, will look at CMEs from two different angles. Tomographic techniques may help to reconstruct the 3D structure of CME features. This may allow for the observation of secondary slow shocks.

In situ satellite observations may also be able to provide more conclusive evidence for secondary slow shocks than coronagraph observations. It would certainly be interesting to reinvestigate the old HELIOS data in this respect. The satellite, however, would have to be located in the low-β region close to the sun in order to be able to observe the slow shocks, because presumably the secondary slow shock would disappear as the CME moves out into upstream plasma with a high plasma β. Signatures of the secondary slow shock may remain present for later times in the possibly nearly self-similar further expansion of the CME [50]. Unfortunately no missions have been planned for the near future which would provide in situ measurements close enough to the sun. At present the coronal magnetic field cannot directly be measured. When such measurements would become available, this would certainly be a big help for the interpretation of structures in coronagraph images.

It seems that our simulation results on magnetically dominated shock topology stand a better chance of getting observational confirmation in the context of the earth's bow shock flow than in the context of solar CMEs, at least for the near future. This is discussed in the next Section.

8.2 Slow shocks in the earth's magnetosheath

We begin this Section with a brief discussion of the properties of the solar wind, the earth's magnetosphere and magnetic clouds, followed by a presentation of simulation results which show that slow shocks can be present in the earth's magnetosheath following the bow shock under magnetically dominated solar wind conditions for which switch-on shocks occur. Then we discuss observational evidence for the presence of slow shocks in the earth's magnetosheath. A preliminary discussion of some of the simulation results described in this Chapter has been presented as a brief report [153]. A more complete account will appear in [154].

8.2.1 The solar wind, the earth's magnetosphere and magnetic clouds

Fig. 8.4 shows solar wind parameters measured by the ACE satellite [156] in front of the earth's bow shock during the full month of February 1999. The solar wind plasma β is most often larger than one but has a large variation (the axis is logarithmic). The (total) sonic and Alfvénic Mach numbers are high (often higher than ten), so the (total) dynamic pressure is generally large compared to the magnetic and thermal pressures. The ecliptic plane is the plane in which the earth orbits around the sun. On average the solar wind magnetic field — or Interplanetary Magnetic Field (IMF) — is expected to lie in the ecliptic plane and to make an angle θ_B of approximately 45° with the sun-earth line [67]. This angle is due to the spiraling of the magnetic field lines rooted in the rotating sun, an effect that can be seen for instance in the model flow of Fig. 5.12. It can be seen in Fig. 8.4 that the angle θ_B often deviates substantially from the value of 45°. The angle θ_v between the solar wind velocity and the sun-earth line is generally quite small, less than 5° or so (see Fig. 8.6).

Fig. 8.5 shows a sketch of the earth's magnetic environment. The earth has an intrinsic magnetic field which is roughly a dipole with axis perpendicular to the ecliptic plane, and which is confined to a region called the *magnetosphere*. The supersonic and super-Alfvénic (and thus superfast) solar wind forms a bow shock in front of the earth. The region just downstream from the bow shock is called the magnetosheath, which

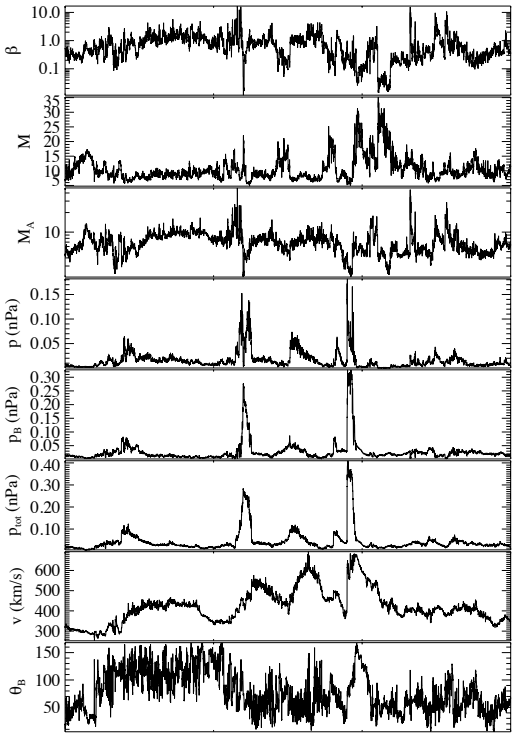

Figure 8.4: *ACE solar wind data for the full month of February 1999. p_{tot} and p_B are the total and the magnetic pressure respectively, and θ_B is the angle between the magnetic field and the sun-earth line.*

is separated from the magnetosphere by a contact surface called the *magnetopause*. In coordinate systems generally used in magnetospheric physics, the sun-earth line is the x-axis, the ecliptic plane is the xy plane and the z-axis is perpendicular to the ecliptic plane. The orientation of the z-axis is chosen such that the earth's magnetic field has a positive B_z component.

When the magnetosheath magnetic field in front of the magnetopause lies in the ecliptic plane, — in the direction perpendicular to the paper in Fig. 8.5 —, then it is oriented perpendicular to the earth's dipole field, such that at the dayside magnetopause the two fields do not reconnect. Positive B_z magnetosheath field has the same orientation as the earth's field, such that again reconnection is not enhanced. For negative B_z magnetosheath field, however, the two fields are anti-parallel such that magnetopause reconnection is strongly enhanced. This increased reconnection enhances the energetic coupling between the solar wind and the

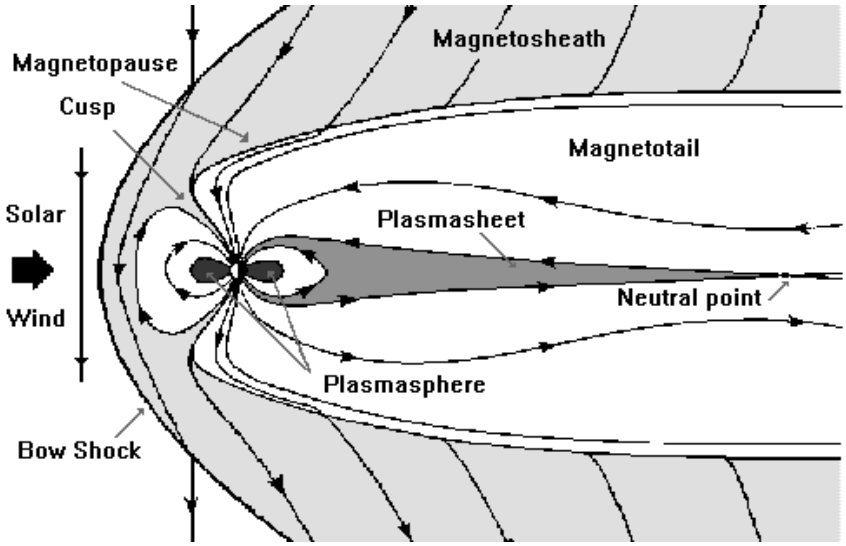

Figure 8.5: *The earth's magnetic environment (xz plane). (courtesy ISPEC)*

magnetosphere, which leads to magnetic storms. It is believed that there is a direct relation between the IMF orientation, as measured upstream from the bow shock, and the orientation of the magnetosheath magnetic field in front of the magnetopause at later times. It is thus said that magnetic storms occur when the IMF has a large negative B_z component for an extended period of time.

A magnetic cloud is a transient ejection in the solar wind defined by relatively strong magnetic fields, a smooth rotation of the magnetic field direction and a low plasma β [15]. Fig. 8.6 shows WIND satellite data describing a magnetic cloud arriving at the earth in January 1997 [15]. The dotted line indicates the arrival of the magnetic cloud, which is preceded by a fast shock. B_z turns gradually from strongly negative to strongly positive during the 22 hours that the cloud event lasts. The cloud is interpreted to be the magnetic flux rope which forms the cavity in the pre-CME structure of Fig. 8.1, while the high-pressure material at the trailing edge of the cloud is believed to be prominence material [15]. The persistent strong negative B_z magnetic field introduced by the magnetic cloud of Fig. 8.6 caused a magnetic storm of moderate strength through enhanced magnetic reconnection at the magnetopause. These conceptual scenarios are generally accepted often mainly based on correlation analysis arguments, but the physical mechanisms of how a magnetic cloud precisely leads to a magnetic storm remain largely un-

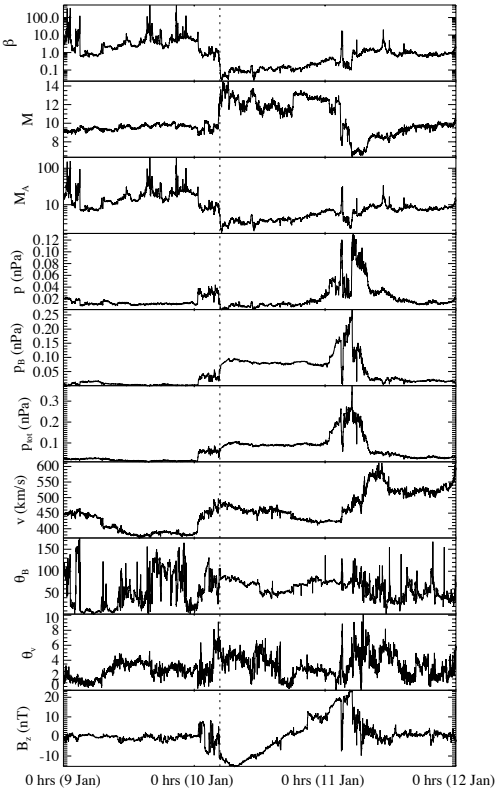

Figure 8.6: *WIND data describing a magnetic cloud arriving at the earth in January 1997. θ_v is the angle between the velocity and the sun-earth line. The dotted line indicates the arrival of the magnetic cloud, which is thought to be a flux rope. In the magnetic cloud the magnetic field dominates, such that the plasma β is low. The cloud is preceded by a fast shock, and is followed by high-pressure material, which is thought to originate from a solar prominence.*

known. For instance, it is not well known how and how fast the negative B_z field of the magnetic cloud propagates through the magnetosheath and reaches the magnetopause.

8.2.2 3D bow shock flows around a paraboloid surface

This Section describes 3D MHD simulations which model the interaction of the solar wind with the earth. The flow of the solar wind around the

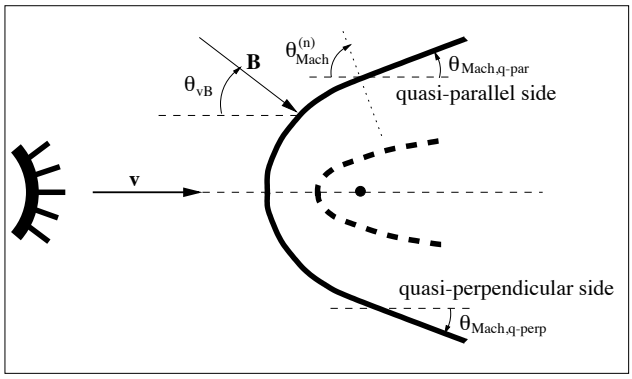

Figure 8.7: *Sketch of the simulation set-up for the problem of solar wind flow around the earth. We model the magnetopause (thick dashed) as a conducting paraboloid. The bow shock is thick solid.* $\theta_{Mach,q-par}$ *is the Mach angle on the quasi-parallel side of the bow shock, where the magnetic field is close to parallel to the shock normal.* $\theta_{Mach,q-perp}$ *is the Mach angle on the quasi-perpendicular side.* $\theta^{(n)}_{Mach}$ *is the normal Mach angle on the quasi-parallel side.*

earth can best be modeled taking into account the inner magnetosphere and the ionosphere — see e. g. [122] and references therein —, but we are primarily interested in investigating the bow shock and the flow in the magnetosheath behind the bow shock, so we can as a first approximation study the flow around a perfectly conducting paraboloid surface which models the magnetopause [174, 16] (Fig. 8.7). This approximation implies that the process of magnetic reconnection at the magnetopause is not considered in our simulations. The solar wind flow is most of the time almost radial along the sun-earth line, so for simplicity we align the velocity of the incoming plasma with the sun-earth line and with the symmetry axis of the paraboloid. In our simulations we consider a uniform upstream flow in which the magnetic field $\vec{B}$ makes an angle θ_{vB} with the velocity $\vec{v}$. For definiteness we think of the magnetic field as lying in the ecliptic plane, but a field rotated out of that plane would simply make the solutions presented below rotate around the sun-earth line. This flow problem has three independent free upstream parameters, for which we choose the Mach number in the direction of the incoming flow $M = v/c$, the plasma $\beta = 2p/B^2$, and the angle θ_{vB}. As before we simulate the 3D bow shock flows starting from a uniform initial condition and by advancing the time-dependent MHD equations until a steady state solution is reached. The simulations are performed on stretched polar-like structured grids with $30 \times 60 \times 30$ or $60 \times 120 \times 60$ cells.

We are interested in the influence of intrinsically magnetic effects on the bow shock and magnetosheath flow, so we start out with a discussion of bow shock flows with magnetically dominated solar wind parameters for which switch-on shocks occur, followed by a discussion of bow shock flow simulations for pressure-dominated parameter values.

The reader will notice many similarities between the simulation results to be presented in this Section for 3D bow shock flows around a paraboloid surface, and the results for flow around a sphere which were presented in Chap. 7. This is not surprising, because it confirms the argumentation in Chap. 7 that the results on magnetically dominated bow shock topology are generic and do not depend on the shape of the obstructing obstacle.

Magnetically dominated bow shock flows

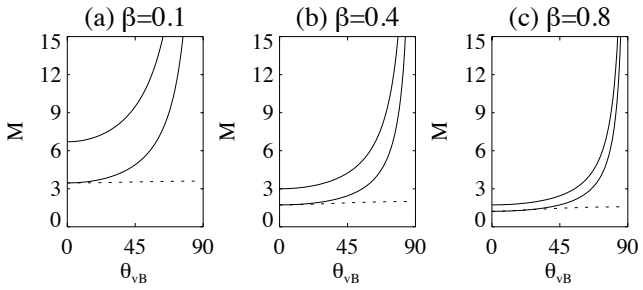

Figure 8.8: *Magnetically dominated parameter regime (switch-on shocks occur) for various values of β. For given plasma β and angle θ_{vB}, switch-on shocks can arise for (total) Mach numbers between the two solid lines.*

As was described in Chap. 3, the occurrence of switch-on shocks is an intrinsically magnetic effect which can only arise in a certain regime for the upstream parameters. At a point on a shock front where the magnetic field is perpendicular to the shock front — we call such a point a perpendicular point —, the shock is switch-on when the upstream Alfvénic Mach number M_{An} in the direction n normal to the shock surface — and thus along the incoming magnetic field — satisfies [80, 150]

$$1 < M_{An} < \sqrt{\frac{\gamma(1-\beta)+1}{\gamma-1}}. \tag{8.1}$$

Switch-on shocks cannot arise for $\beta > 2/\gamma = 1.2$.

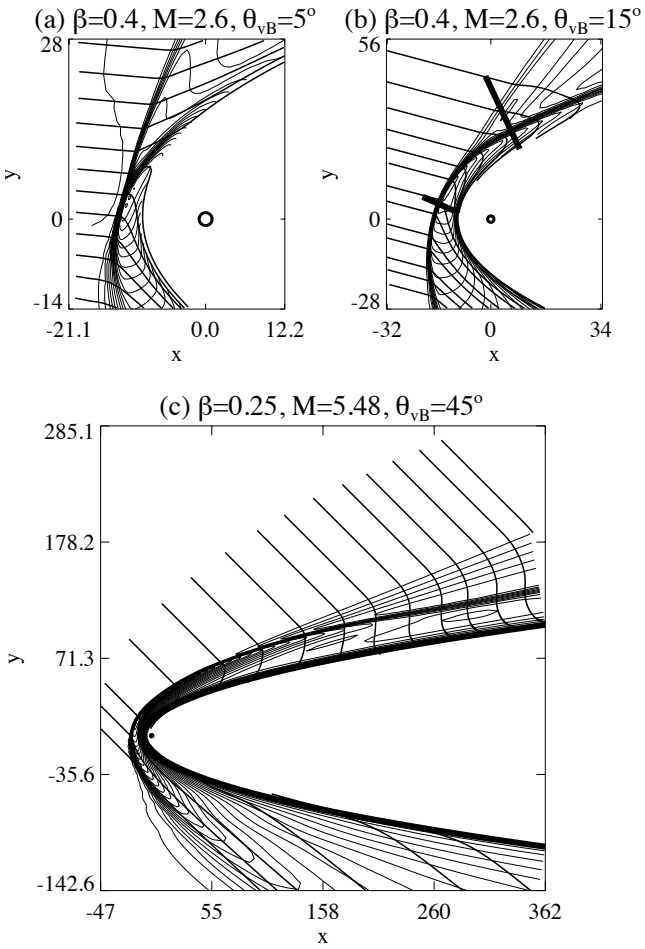

Figure 8.9: *3D bow shock flows around a paraboloid surface for magnetically dominated upstream parameter values. Density contours and magnetic field lines in the ecliptic plane are shown. In all flows a slow shock is following the leading shock.*

It follows from Eq. 8.1 that the condition for the occurrence of switch-on shocks in the configuration of Fig. 8.7 can be written as

$$M_- = \frac{1}{\cos\theta_{vB}}\sqrt{\frac{2}{\gamma\beta}} < M < M_+ = \frac{1}{\cos\theta_{vB}}\sqrt{\frac{2}{\gamma\beta}}\sqrt{\frac{\gamma(1-\beta)+1}{\gamma-1}}, \quad (8.2)$$

with the total Mach number $M = v/c$ and v the magnitude of the

velocity. In Fig. 8.8 the switch-on parameter regime in the θ_{vB}–M plane is plotted for various values of β. For a given value of θ_{vB}, switch-on shocks can arise for values of M between M_- and M_+ (corresponding to the two solid lines). The Mach number has to be higher than $M_0 = c_f/c$ (dotted line), with c_f the fast MHD speed along the sun-earth line, because the inflow along the sun-earth line has to be superfast in order to have a fast leading shock. The limit $M = M_-$ corresponds to $\theta_{vB} = \theta^{(n)}_{Mach}$ (Fig. 8.7). For $M < M_-$, the normal Mach angle $\theta^{(n)}_{Mach}$ is smaller than the angle θ_{vB}, such that there is no perpendicular point on the shock front.

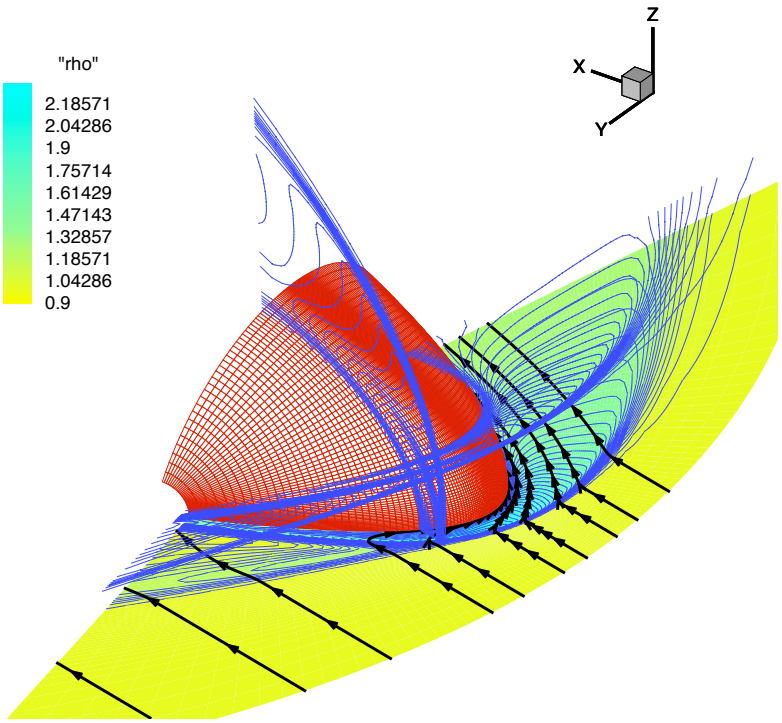

Figure 8.10: *3D bow shock flow around a paraboloid surface with inflow* $\beta = 0.4$, $M = 2.6$, *and* $\theta_{vB} = 15°$. *This is the simulation of Fig. 8.9b. Density contours and field lines are shown in the ecliptic plane — the* xy *plane — , and density contours in two additional planes. The leading shock front is clearly followed by a secondary shock front, which is attached to the leading front, and which extends well out of the ecliptic plane. The secondary shock front is of the slow type.*

Fig. 8.9 shows the results of three 3D bow shock simulations with magnetically dominated upstream parameter values (switch-on shocks arise, Eq. 8.2). Density contours and magnetic field lines are shown in the ecliptic plane. Units are expressed in earth radii R_E, and the approximate size and location of the earth is indicated by a circle in the origin of the coordinate system. The distance between the earth and the magnetopause is taken as $10\,R_E$ along the sun-earth line, and $17\,R_E$ in the direction perpendicular to this line. In all three flows a slow shock is following the leading shock and is attached to it. Intrinsically magnetic effects thus substantially modify the flow topology compared to the single-front bow shock solution which arises for a pressure-dominated upstream flow. We have performed many more simulations with parameter values in the switch-on regime (Eq. 8.2), and in the resulting flows we have always obtained the same basic flow topology, with a secondary slow shock front following the leading front and attached to it. This is the topology of Fig. 7.5b, which has been explained in terms of the properties of MHD shocks in Sec. 7.1.3.

A 3D visualization of the flow of Fig. 8.9b is shown in Fig. 8.10. Fig. 8.11 shows how streamlines and magnetic field lines originating from points slightly above the ecliptic plane drape around the paraboloid obstacle. It is clear that the presence of the secondary slow shock greatly influences the field line draping, as the magnetic field is refracted strongly at the slow shock front. This change in field line topology may influence the reconnection process at the earth's magnetopause. Fig. 8.12 shows how the secondary shock front is curved. The surface drawn is an isosurface of $||\nabla\rho||$, which wraps around the shock surfaces where $||\nabla\rho||$ peaks. A cut-off value $c_{cut-off}$ is chosen which defines the iso-surface $||\nabla\rho|| = c_{cut-off}$ drawn. A smaller cut-off value would lead to an iso-surface with larger spatial extent. The shock surfaces thus actually extend further than one would infer from Fig. 8.12.

In Fig. 8.9, the way in which the magnetic field is refracted at the secondary shocks shows that those shocks are of the slow type. The slow shocks are almost switch-off shocks, such that the magnetic field is almost parallel to the shock normal downstream from the shock. In Figs. 8.9a and b the slow shock is followed by a strong rarefaction region, in which the magnetic field rotates further. We can determine the types of the shocks more accurately by considering the variation of flow parameters along cuts perpendicular to the shock fronts.

Fig. 8.13 shows such cuts along the thick solid lines perpendicular to slow and intermediate shock segments in Fig. 8.9b. Let us first look at the cut perpendicular to the secondary slow shock, presented in Fig. 8.13a–f. Going from left to right, the density, pressure and magnetic field strength first increase when the leading fast shock is passed. At the second discontinuity, the density and the pressure rise whereas the

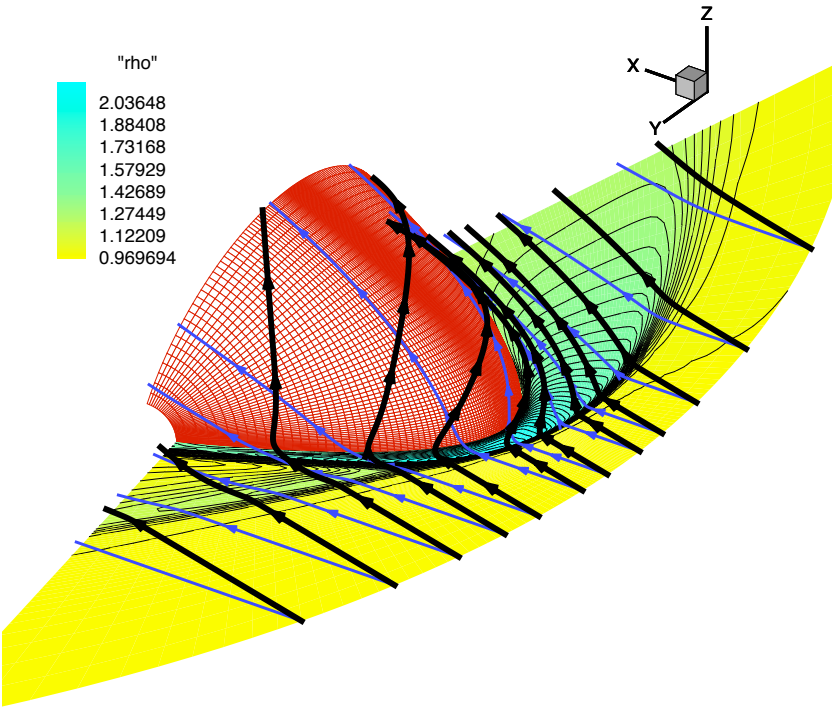

Figure 8.11: *Magnetic field lines (black) and streamlines (blue) for the bow shock flow solution of Fig. 8.9b. The field lines and streamlines are drawn starting from points located slightly above the ecliptic plane, and drape around the paraboloid obstacle in the magnetosheath region.*

magnetic field strength decreases sharply. This is a clear signature of a slow shock. This diagnosis is confirmed by the normal Mach number plots of Fig. 8.13d-f. The flow is superslow but sub-Alfvénic upstream, and subslow downstream. The shock is thus a 3–4 slow shock. The upstream Alfvénic Mach number is very close to one, however, so the shock is very close to a 2=3–4 slow switch-off shock.

In Fig. 8.13g–l we consider the cut perpendicular to the leading shock front in Fig. 8.9b. We cut the leading shock front between the point where the magnetic field is perpendicular to the shock front, and the point where the secondary slow shock is attached to the leading front. The density and pressure increase at the discontinuity, and the component $B^{(t)}$ of the magnetic field tangential to the shock front changes sign. This is a clear signature of an intermediate shock. We can again confirm

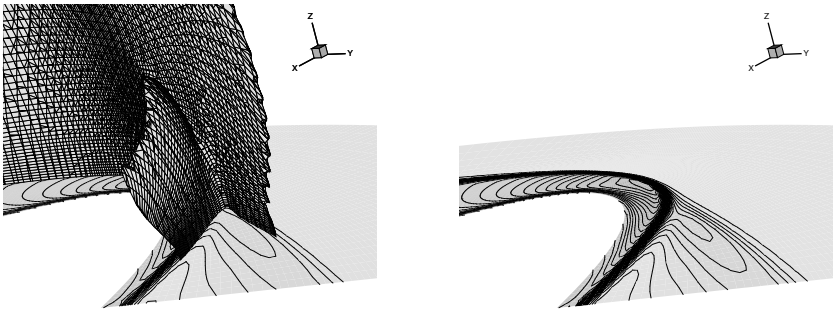

Figure 8.12: *Visualization of the shock fronts for the bow shock flow solution of Figs. 8.9b, 8.10 and 8.11. The secondary slow shock clearly extends out of the ecliptic plane.*

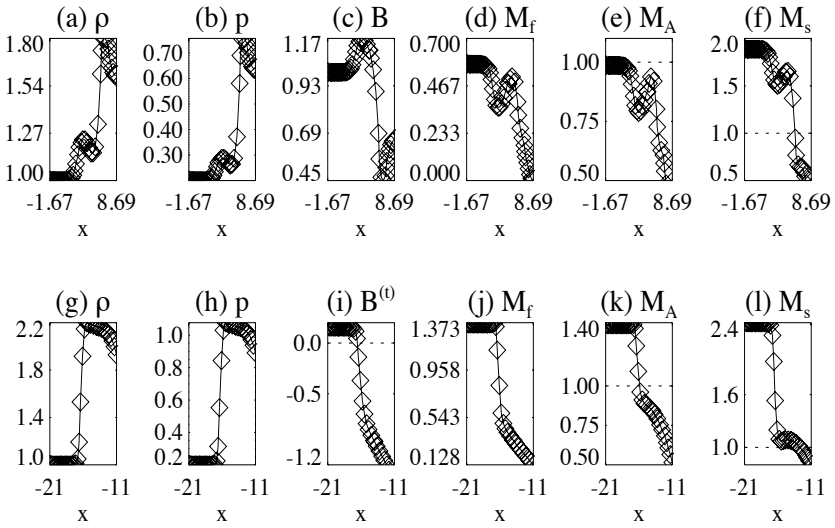

Figure 8.13: *(a–f) Cut along the upper thick solid line in Fig. 8.9b. Going form left to right, we first pas the leading fast shock. The second discontinuity is a 3–4 slow shock, which is very close to a 2=3–4 slow switch-off shock. (g–l) Cut along the lower thick solid line in Fig. 8.9b. The shock is a 1–3 intermediate shock, which is very close to a 1–3=4 intermediate shock.*

this diagnosis by looking at normal Mach numbers (Fig. 8.13j–l). The flow is superfast (and thus super-Alfvénic) upstream, and sub-Alfvénic but superslow downstream. The shock is thus a 1–3 intermediate shock, but very close to 1–3=4.

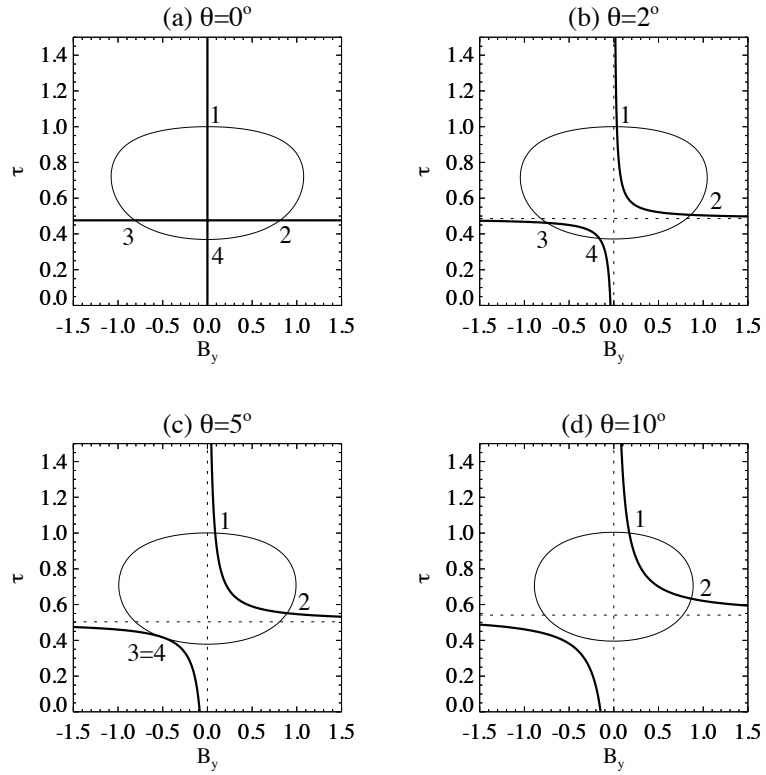

Figure 8.14: *Solutions of the RH relations for the upstream parameters of Fig. 8.9b with* $\theta_{vB} = 15°$. *These parameters are magnetically dominated. The maximum angle between the magnetic field and the shock normal for which intermediate shocks can occur is approximately* 5°.

Fig. 8.14 shows that for the upstream parameter values of Fig. 8.9b the maximum angle between the magnetic field and the shock normal for which the 1–3 intermediate shock can occur is approximately 5°. This is consistent with the angle for which the leading shock front splits up into two consecutive shock fronts in Fig. 8.9b.

The results shown here for 3D flows around a paraboloid surface have the same basic topology as the magnetically dominated flow around a

conducting sphere which was described in Chap. 7. All this indicates that this topology is generic for 3D bow shock flows with magnetically dominated parameter values. The secondary slow shock is required because of the geometrical properties of switch-on shocks, as was argued in Chap. 7. These findings are an important addition to the general theory of MHD bow shocks [114].

Pressure-dominated bow shock flows

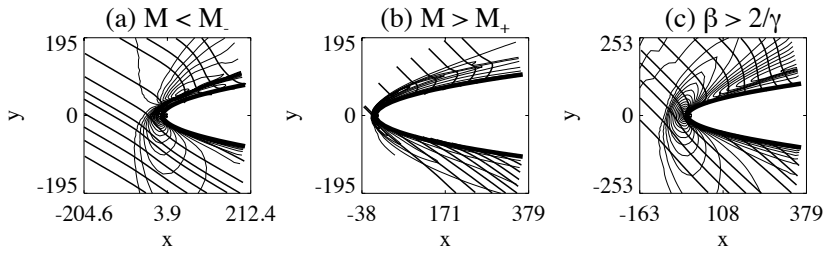

Figure 8.15: *3D bow shock flows around a paraboloid surface for pressure-dominated upstream parameter values (switch-on shocks do not occur). Density contours and magnetic field lines in the ecliptic plane are shown.*

It is interesting to consider bow shock flows in the configuration of Fig. 8.7 for pressure-dominated upstream parameter values for which switch-on shocks do not occur. Indeed, in Fig. 8.15 we present preliminary results of such simulations for which we *do* find secondary shocks behind the leading shock. Based on our discussion of the switch-on parameter regime above (Eq. 8.2), we can distinguish between three different parameter regimes outside the switch-on regime. First there is the case that $\beta > 2/\gamma$. For $\beta < 2/\gamma$, we have the two cases $M < M_-$ and $M > M_+$. As shown in Fig. 8.15, in all of those three regimes we have found secondary shocks for some choices of parameter values, while for most choices of parameter values in these three regimes we did not find secondary shocks. Fig. 8.15a considers a bow shock flow with $M < M_-$ ($\beta = 0.4$, M=1.91, $\theta_{vB} = 30°$). In Fig. 8.15b a bow shock flow with $M > M_+$ is considered ($\beta = 0.25$, M=8.76, $\theta_{vB} = 45°$). Fig. 8.15c shows a bow shock flow with $\beta > 2/\gamma$ ($\beta = 1.5$, M=1.34, $\theta_{vB} = 45°$). The secondary shock is not always attached to the leading shock front. The reader may notice that these preliminary simulations were carried out at low resolution and contain some unexplained features. The need for an extensive parameter study with high resolution simulations is apparent.

On one hand it is surprising to find slow secondary shocks for flows with pressure-dominated upstream parameter values, because in the 2D case slow shocks arise if and only if the upstream flow is magnetically dominated and switch-on shocks occur (Sec. 6.3). On the other hand, it is not so surprising, because in principle every fast shock could be followed by slow or intermediate shocks. For pressure-dominated parameter values, the formation of the secondary slow shock is not related to the geometrical properties of switch-on shocks at perpendicular points on the leading shock front, but instead seems to depend more on the shape of the obstacle and the angle θ_{vB}. The secondary shocks in Fig. 8.15a and c may be due to boundary layer separation. For the case of solar wind flow around the earth, the precise shape of the magnetopause and the reconnection process at the magnetopause may become important in determining if slow shocks in this parameter regime exist or not.

8.2.3 Observations of slow shocks in the magnetosheath

Observations by Song et al. (1992) [141]

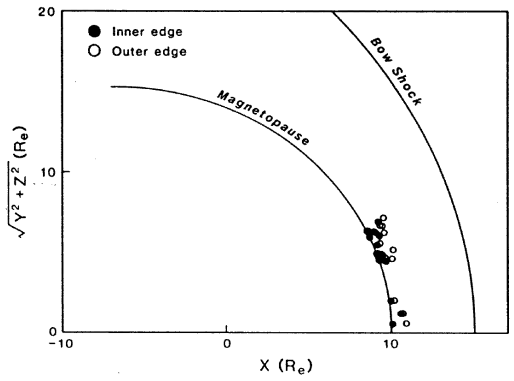

Figure 8.16: *Locations of observed density enhancements in the magnetosheath near the magnetopause. (From Song et al. (1992) [141])*

The results described in the above Section on slow shocks following fast shocks may have direct implications for the structure of the flow in the earth's magnetosheath under some solar wind conditions. Indeed, slow shocks have been observed in the dayside magnetosheath and in the distant magnetotail region.

Song et al. [140, 141, 138] claim the existence of density enhancements

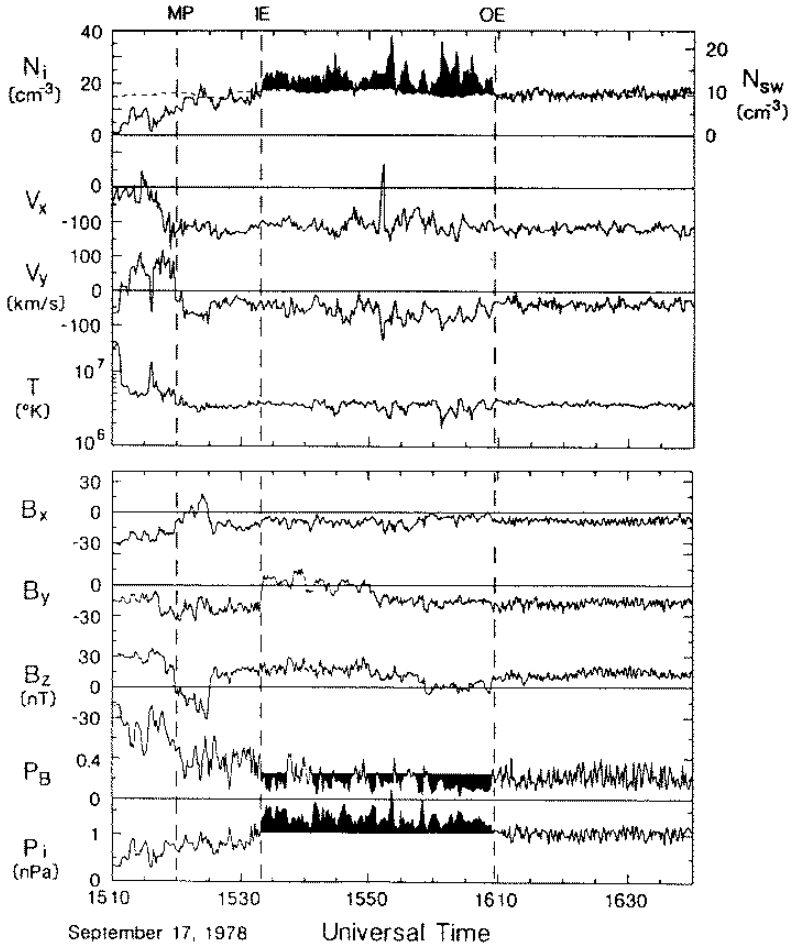

Figure 8.17: *An outbound magnetosheath pass on September 17, 1978, by ISEE2. MP stands for magnetopause, IE for inner edge, and OE for outer edge. The region with enhanced ion density N_i, ion pressure P_i and magnetic pressure P_B is shaded. The magnetosheath flow is disturbed by kinetic waves of various kinds which complicate a clear interpretation. The jump at OE is interpreted as a slow shock, and results of a Rankine-Hugoniot analysis of the shock are presented in Table 8.1. (From Song et al. (1992) [141])*

of slow mode type in front of the dayside magnetopause in more than

50% of ISEE-1 and ISEE-2 satellite passes. The slow mode structures were interpreted as slow shock fronts. Fig. 8.16 shows where the inner and outer edges of the density enhancements were observed between the earth's bow shock and magnetopause close to the sun-earth line. Fig. 8.17 gives an example of an observation of such a density enhancement. The density drop at the inner edge (IE) may be due to the boundary layer effect shown in Fig. 7.9.

As can be seen in Fig. 8.17, the magnetopause flow tends to be disturbed by kinetic waves of various kinds which often complicate a clear interpretation of macroscopic flow structures. For this and other reasons some skepticism has arisen about the interpretation of the observations in [140, 141] as stationary slow shocks.

Indeed, the observed slow mode waves may not be stationary, but may be transient structures. It has been shown in 2D MHD simulations [180] that transient slow mode waves and shocks can be generated by the interaction of various types of solar wind waves with the earth's bow shock and magnetosphere. This has been confirmed in 2D hybrid simulations [97] and in 3D MHD simulations [16]. The relevance of these alternative explanations was questioned in recent work by Song et al. [139, 142]. We have to proceed cautiously and have to keep in mind alternative interpretations, but it seems justified to investigate if at least some of the structures observed by Song et al. may be related to the stationary slow shocks found in our 3D MHD simulations of magnetically dominated bow shock flows.

Table 8.1: *Comparison of upstream and downstream Mach numbers for a slow switch-off shock, a slow shock observed in the earth's magnetosheath (Song et al. (1992) [141]), and the secondary slow shock in the simulation of Fig. 8.9b.*

slow switch-off shock Fig. 3.8e	**Song et al. (1992)** Fig. 8.17	**slow shock** Fig. 8.9b
upstream		
$M_A = 1$	$M_A = 1.17$	$M_A = 0.99$
$M_s > 1$	$M_s = 1.38$	$M_s = 1.6$
downstream		
$M_A = M_s < 1$	$M_A = 0.93$	$M_A = 0.65$
	$M_s = 1.00$	$M_s = 0.65$

First we investigate if the observed and simulated shocks are similar regarding jumps in normal Mach number. Rankine-Hugoniot analysis

of the observed slow shock of Fig. 8.17 leads to upstream Mach numbers $M_A^{(u)} = 1.17$ and $M_s^{(u)} = 1.38$, and to downstream Mach numbers $M_A^{(d)} = 0.93$ and $M_s^{(d)} = 1.00$ [141]. Note that these Mach numbers are taken in the direction normal to the slow shock front, but that we have dropped the subscript n here. In Table 8.1 these values are compared with the Mach numbers of a slow switch-on shock, for which $M_A^{(u)} = 1$ and $M_s^{(u)} > 1$, and $M_A^{(d)} = M_s^{(d)} < 1$. It turns out that the secondary slow shock in Fig. 8.9b has Mach numbers in a similar range: $M_A^{(u)} = 0.99$ and $M_s^{(u)} = 1.6$, and $M_A^{(d)} = 0.65$ and $M_s^{(d)} = 0.65$. This suggests that at least some of the slow shocks observed by Song et al. may be of the same type and origin as the slow shocks in Fig. 8.9.

Second we investigate if the solar wind has parameter values in the switch-on regime often enough to explain secondary slow shocks in the dayside magnetosheath in 50% of ISEE-1 and ISEE-2 passes. It turns out that this cannot be the case, because the solar wind often has a high plasma β and/or high Mach numbers (Fig. 8.4). We have made an analysis of three arbitraryly chosen months of ACE [156] solar wind satellite data (July 1998, and January and February 1999) and have found that for each of these months the solar wind averaged over five-minute time-intervals was magnetically dominated (switch-on shocks occur, Eq. 8.2) for about 8% of the time (7.0% for June 1998, 7.8% for January 1999, and 7.7% for February 1999). This is clearly not enough to explain stationary slow shocks in the dayside magnetosheath in more than 50% of the cases, as reported in [141], especially if one realizes that the solar wind is often quite oscillatory and that it may not often reside in the switch-on regime long enough for the slow shock to form as a stationary feature. However, we have found that several times per month the solar wind seems to reside in the switch-on regime for half an hour or more. This can be seen from the solar wind histogram plots of Fig. 8.18. Estimates of the dynamical response time of the magnetosheath flow indicate that the slow shock could be formed in a time span of half an hour. This has to be confirmed in future time-dependent MHD simulations which take into account the rather erratic behavior of the solar wind.

Based on our investigation of the solar wind parameters, we can thus expect that several times per month well-formed stationary slow shocks exist in the earth's magnetosheath. During short intervals amounting to 8% of the total time the solar wind is temporarily in the switch-on regime and the magnetosheath flow is probably disturbed such that slow shocks start to form, but stationarity of the slow shocks is presumably not attained.

Slow shocks of the type present in our simulation results for magnetically dominated parameter values may thus explain part of the observations done by Song et al. [141]. We can speculate that the existence

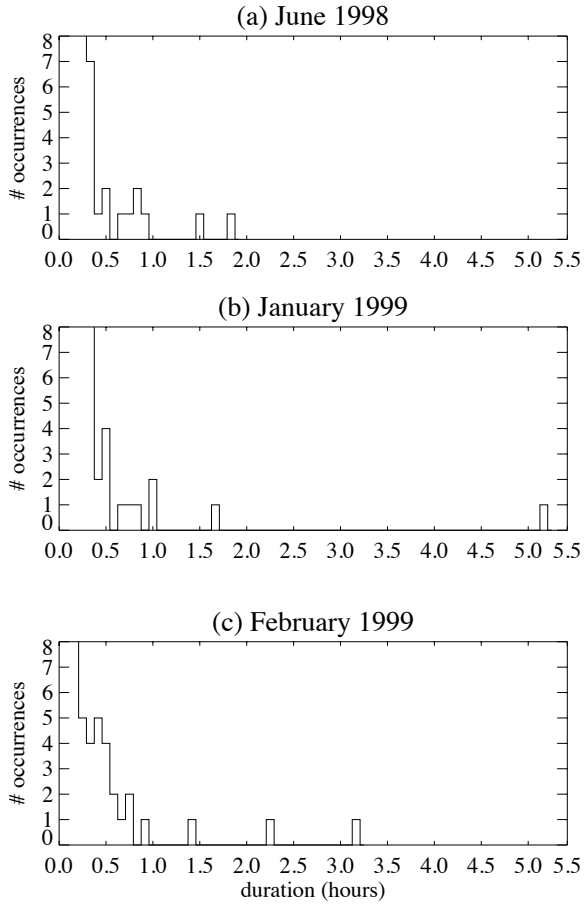

Figure 8.18: *Histograms for three months of ACE solar wind data. Several times per month the solar wind is in the switch-on regime for a period longer than 0.5 hours.*

of secondary shocks for certain parameter values not in the switch-on regime may partially explain why Song et al. observed secondary slow shocks in more than 8% of ISEE-1 and ISEE-2 magnetosheath passes. It is hard to quantify this effect, however, because our discussion in Sec. 8.2.2 indicated that the occurrence of secondary shocks outside the switch-on regime seems not to be systematic.

Third we look at the location in the magnetosheath where the slow shocks are present in our simulation results. Given the observational fact that the solar wind is most often a high Mach number flow (Fig. 8.4),

we can see from Fig. 8.8 that secondary slow shocks are more likely to occur for relatively large angles θ_{vB}. Fig. 8.9 shows clearly that the point where the secondary slow shock is attached to the leading fast shock, shifts tailwards when θ_{vB} increases. The secondary shock is then not present in the dayside magnetosheath close to the sun-earth line, where the shocks studied in [141] were encountered. However, in [141] it is mentioned that slow shocks were also found in the flanks of the magnetosheath. Slow shocks have also been reported in the distant magnetotail region [38, 37], and the secondary shocks present in our simulation results may be related to these observed slow shocks. These slow shocks may alternatively be due to magnetic reconnection in the magnetotail (Fig. 2.15).

We may thus conclude that our simulation results for bow shock flows with magnetically dominated upstream parameters offer a physically attractive explanation for the possible observation of stationary slow shocks in the magnetosheath. Some of the slow shock observations by Song et al. [141] may be explained by our simulation results, but certainly not all. Our simulation results make some clear predictions about when and where slow shocks could be observed, and it would be interesting to re-investigate the observational data in this respect. Slow shocks should be observed preferably when $\beta < 2/\gamma$ and θ_{vB} is large in the solar wind, and only on the quasi-parallel side of the magnetosheath and not too far from the symmetry plane containing the inflow magnetic field.

Global reconfiguration of the magnetosheath flow during magnetic cloud events and the mechanism and timing of magnetic storms

The solar wind is often low-β for a substantial time when a magnetic cloud hits the earth's magnetic environment. Indeed, for instance in the magnetic cloud event of January 1997 (Fig. 8.6) [15] the plasma β was approximately equal to 0.1 for about 22 hours, with a Mach number $M \sim 12$ and $\theta_{vB} \sim 70°$. This flow is magnetically dominated (switch-on shocks occur, Eq. 8.2). We have performed a simulation with these parameter values (Fig. 8.19a), and have found a secondary slow shock and the topology of Fig. 7.5b. This indicates that during this event a slow shock may have been formed in the magnetosheath in the direction of the magnetotail on the quasi-parallel side of the magnetosheath. It seems thus that secondary slow shocks in the magnetosheath are likely to be formed during magnetic cloud events because of the low-β nature of magnetic clouds and because of large angles θ_{vB}. Fig. 8.19b–d shows what a satellite which crosses the magnetotail would observe when such a secondary slow shock were to be present. It would be interesting to

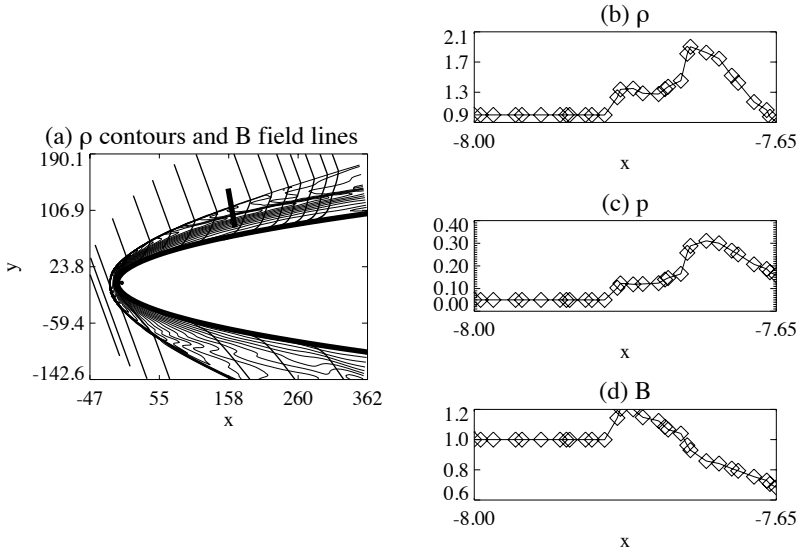

Figure 8.19: *3D bow shock flow around a paraboloid surface with inflow* $\beta = 0.1$, $M = 12$, *and* $\theta_{vB} = 70°$. *These are the parameter values in the magnetic cloud of Fig. 8.6, and they lie in the switch-on regime. (a) The leading shock front is clearly followed by a secondary shock front, which is attached to the leading front. (b–d) A satellite passing through the magnetosheath in the tail region on the quasi-parallel side — along the thick line in (a) — would observe a slow shock following a fast shock.*

investigate the observational data and to look for signatures of slow shocks during magnetic cloud events.

In the solar wind thermal and dynamic pressure effects normally dominate over magnetic effects, and the magnetosphere is generally in dynamic equilibrium with this pressure-dominated solar wind. During the magnetic cloud event of Fig. 8.6, however, the solar wind abruptly becomes low-β and the angle θ_{vB} becomes large, such that intrinsically magnetic effects become dominant. When a magnetic cloud arrives, the magnetosphere has to adjust to the now magnetically dominated solar wind on short time scales.

This adjustment involves a temporary global reconfiguration of the magnetosheath flow from a pressure-dominated single-front bow shock flow topology to a magnetically dominated topology with a secondary slow shock. We can speculate that this temporary global reconfiguration may have a profound influence on the mechanism of magnetic storms and on the timing of magnetic storm onset in the following ways.

Fig. 8.9b shows that in the magnetically dominated bow shock topology the field lines at the magnetopause are highly elongated and stretch out around a large part of the dayside magnetopause. In the case of negative B_z magnetosheath field, this may change the location where reconnection occurs, and increased field strength at the magnetopause may increase the rate of reconnection. In Fig. 8.12 one can see that the slow shock front has a limited spatial extent which is centered around the plane of the incoming magnetic field. The magnetic field rotates slowly during a magnetic cloud event, and if a slow shock would be formed, then this slow shock front would presumably rotate in the magnetosheath along with the rotating cloud field, thus influencing the reconnection location.

These effects may influence the storm mechanism and intensity. Solar wind perturbations which introduce a certain amount of negative B_z and which reconfigure the magnetosheath because they are magnetically dominated, may cause more severe storms — it is said that they are more *geo-effective* — than perturbations which introduce the same amount of negative B_z but do not reconfigure the magnetosheath flow because they remain pressure-dominated. If this is true, then the plasma β and the angle θ_{vB} may be important indicators for geo-effectiveness, next to B_z.

It is generally believed that geo-effective magnetic clouds introduce magnetic field with a negative-B_z component into the magnetosheath which, upon arrival at the magnetopause, leads to enhanced reconnection with the earth's positive-B_z magnetic field and thus causes a magnetic storm. It is not well understood how and how fast this negative-B_z field reaches the magnetopause. Our simulation results suggest that magnetic clouds would not simply *propagate through* the magnetosheath, as is often believed [130], but could rather cause a *global reconfiguration* of the magnetosheath flow involving a slow shock. When a magnetic cloud arrives at the bow shock and a slow shock forms, the characteristic time of this global reconfiguration of the magnetosheath may determine when negative B_z reaches the magnetopause, and may thus influence the timing of magnetic storm onset. This may explain the time delay which is observed between the measurement of negative B_z IMF in front of the bow shock and the arrival of negative B_z field at the magnetopause. This time delay cannot be explained as a simple propagation effect.

These scenarios remain speculative for now, but it would certainly be interesting to investigate them more closely in time-dependent numerical simulations, and to look for observational signatures which would confirm them. The important role of reconnection has to be considered explicitly as well. In the near future the CLUSTER mission will provide us with detailed observations of the dayside magnetosheath region, which may confirm the existence of slow shocks in the magnetosheath for magnetically dominated solar wind conditions.